Quantitative Microwave Imaging Based on a Huber regularization

Funing Bai, Wilfried Philips and Aleksandra Pižurica

Department of Telecommunications and Information Processing (IPI-TELIN-iMinds)

Ghent University, Belgium

Abstract—**Reconstruction of inhomogeneous dielectric objects from microwave scattering by means of quantitative microwave tomography is a nonlinear, ill-posed inverse problem. In this paper, we employ the Huber function as a robust regularization approach for this challenging problem. The resulting reconstructions both in 2D and 3D from sparse data points for piecewise constant objects are encouraging. The reconstructions of more complex permittivity profiles from breast phantom data indicate potential for use in biomedical imaging.**

I. Introduction

Microwave imaging relies on the capability of microwaves to differentiate among different materials/tissues based on the contrast in their dielectric properties. Quantitative microwave tomography aims at estimating the permittivity profile of a scattering object based on measured scattered fields. Recent research [1]–[7] indicates potentials of quantitative microwave tomography to discriminate between tumors and healthy tissue in breast imaging. Considerations of safety, cost, availability, sensitivity and specificity are in favor of using microwaves for routine medical screening (such as breast cancer screening). One of the main problems is the considerable computational complexity stemming from the difficult, nonlinear inverse problem. Choosing the right regularization strategy is crucial for improving the accuracy of reconstructions as well as for reducing the computational load.

Earlier regularized iterative methods to solve this nonlinear and ill-posed inverse problem include Multiplicative Smoothing [8] (Tikhonov regularization applied in a multiplicative fashion), total variation (TV) [9], edge preserving models [10], [11] and Value Picking (VP) [12]. Edge preserving regularization was imposed on the real and imaginary part of the complex permittivity separately in [10], [11]. Krylov subspace methods were used in [13] and a soft-prior regularization strategy was employed in [14] for microwave imaging in medical applications. A time-domain-based algorithm based on broadband microwave measurements for biological tissues was investigated in [15]. Most of these methods work well on particular classes of permittivity profiles (e.g. TV and VP are well suited for piece-wise constant profiles). Approaches based on Tikhonov regularization or multiplicative smoothing tend to oversmooth the result. Only the models that are able to adapt to discontinuities can yield edge-preserving regularization. While discontinuity-adaptive Markov Random Field (MRF) models have been largely studied in the domain of real functions, their extensions to the complex domain are scarce. For example, edge preserving regularization of [10], [11] was applied to the real and imaginary part of the complex permittivity profile separately.

We proposed a discontinuity adaptive MRF-based regularization in [16] using the robust Huber function. The Huber function

$$g_{Huber}(\eta) = \begin{cases} \eta^2 & |\eta| \leq \gamma \\ 2\gamma|\eta| - \gamma^2 & else \end{cases} \qquad (1)$$

is quadratic for small values of η and linear for large values, avoiding in this way over-smoothing at true discontinuities. In [16], we evaluated this robust regularizer only on simulated 3D piecewise constant objects. In this paper, we evaluate the whole approach not only on different piecewise constant objects but also in a challenging case study with biomedical data. The results demonstrate the effectiveness of the proposed Huber regularization in imaging piecewise constant objects as well as in biomedical imaging. In particular, the results on simulated breast phantom data indicate potentials for applications like breast cancer screening.

This paper is organized as follows. Section II introduces the electromagnetic inverse scattering problem and Gauss-Newton optimization. The proposed method is presented in Section III and results from numerical experiments are shown in Section IV. Conclusions are formulated in Section V.

II. Inverse problem

We consider an unknown object with complex permittivity $\varepsilon(\mathbf{r}) = \varepsilon'(\mathbf{r}) + j\varepsilon''(\mathbf{r})$ embedded in free space ε_0 and illuminated successively with different known time-harmonic incident fields. The discretized unknown permittivity profile $\varepsilon = [\varepsilon_1, \cdots, \varepsilon_\nu, \cdots, \varepsilon_{N^\varepsilon}]$ is estimated iteratively, on a grid with N^ε cube cells within a reconstruction domain $\mathcal{D}$, alternating between the forward and the update problem. The forward problem simulates the scattered electric field for a guessed permittivity profile, using a volume integral equation solver [17]. The scattered fields $\mathbf{e}^{scat}(\varepsilon)$ collected by a number of receiving antennas in the simulation are compared with the measured fields $\mathbf{e}^{meas}$. Based on the resulting error, the permittivity profile is updated. This inverse problem is typically optimized by minimizing a cost function

$$F(\varepsilon) = F^{LS}(\varepsilon) + \mu F^D(\varepsilon) \qquad (2)$$

where $F^{LS}(\varepsilon)$ is the least squares cost function, which evaluates the data error and $F^D(\varepsilon)$ is a regularization term, with

Algorithm 1 The complete algorithm for reconstructing ε

Require: ε_{init}, μ, γ
Ensure: Objects, configuration

$\quad \varepsilon_0 \leftarrow \varepsilon_{init}$
$\quad$ Measure $\mathbf{e}^{meas}$, compute $\lambda^2 = \mu\|\mathbf{e}^{meas}\|^2$
$\quad$ **repeat**
$\quad\quad$ Compute $\mathbf{e}^{scat}(\varepsilon)$
$\quad\quad$ **if** $\dfrac{\|\mathbf{e}^{meas} - \mathbf{e}^{scat}(\varepsilon)\|^2}{\|\mathbf{e}^{meas}\|^2} < 10^{-3}$ **then**
$\quad\quad\quad$ **return** ε
$\quad\quad$ **else**
$\quad\quad\quad$ Compute $\mathbf{J}_k$: $J_{dl} = \partial e_d^{scat}/\partial \varepsilon_l$
$\quad\quad\quad$ Compute Ω_k^{D*} and Σ_k^D using (6-8)
$\quad\quad\quad$ Compute $\Delta\varepsilon_k$ using (4)
$\quad\quad\quad$ Compute β_k with line search
$\quad\quad\quad$ $\varepsilon_{k+1} = \varepsilon_k + \beta_k\Delta\varepsilon_k$
$\quad\quad$ **end if**
$\quad$ **until** k=The number of maximum iterations
$\quad$ **print** ε

---

the parameter $\mu \geq 0$. The least square cost function is

$$F^{LS}(\varepsilon) = \frac{\|\mathbf{e}^{meas} - \mathbf{e}^{scat}(\varepsilon)\|^2}{\|\mathbf{e}^{meas}\|^2} \quad (3)$$

where $\mathbf{e}^{meas}$ and $\mathbf{e}^{scat}(\varepsilon)$ are N^d-dimensional vectors that contain the data for all combinations of illuminating and receiving antennas.

We consider minimization by an approximate line search along a modified Gauss-Newton descent direction, which requires a positive definite Hessian matrix. The complex permittivity in iteration k is updated as $\varepsilon_{k+1} = \varepsilon_k + \beta_k\Delta\varepsilon_k$, where β_k is calculated from line search [18] and $\Delta\varepsilon_k$ is obtained from

$$(\mathbf{J}_k^H\mathbf{J}_k + \lambda^2\Sigma_k^D)\Delta\varepsilon_k = -(\mathbf{J}_k^H[\mathbf{e}^{scat}(\varepsilon_k) - \mathbf{e}^{meas}] + \lambda^2\Omega_k^{D*}) \quad (4)$$

where $(.)^H$ stands for Hermitian transpose and $(.)^*$ denotes the complex conjugate. The trade-off parameter λ is given by $\lambda^2 = \mu\|\mathbf{e}^{meas}\|^2$ [12]. $\mathbf{J}$ is the $N^d \times N^\varepsilon$ Jacobian matrix, which contains the derivatives of the scattered field components with respect to the optimization variables: $J_{d\nu} = \partial e_d^{scat}/\partial\varepsilon_\nu$; Ω_k^{D*} is an $N^\varepsilon-$dimensional vector that contains the derivatives of the regularizing function, $\Omega_\nu^{D*} = \partial F^D/\partial\varepsilon_\nu^*$; Σ_k^D is a $N^\varepsilon \times N^\varepsilon$ matrix, $\Sigma_{\nu,\nu'}^D = \partial^2 F^D/\partial\varepsilon_{\nu'}\partial\varepsilon_\nu^*$. In the following, the subscript k is omitted. The factor $\mathbf{J}^H\mathbf{J} + \lambda^2\Sigma^D$ is known as a modified Gauss-Newton Hessian matrix. To avoid ill-conditioning of the forward problems, constraints are imposed on the real and imaginary parts of the complex permittivity and implemented by a modified, constrained line search [12].

III. Huber regularized reconstruction algorithm

We define the regularization function $F^D(\varepsilon)$ as

$$F^D(\varepsilon) = \frac{1}{2}\sum_\nu\sum_{\nu'\in N_\nu} g_{Huber}(|\varepsilon_\nu - \varepsilon_{\nu'}|) \quad (5)$$

with g_{Huber} defined in (1). The index ν' denotes a spatial position neighboring ν in the neighborhood system N_ν. In 2D, ν is a pair of indices $\nu \equiv (i,j)$ and in 3D a triplet $\nu \equiv (i,j,k)$. We use 8 neighbors in 2D and 26 neighbors in 3D as a compromise between reconstruction quality and complexity. Taking into account that we use a complex Huber function where ε in (5) is a complex number and hence $|\varepsilon_l - \varepsilon_{l'}|^2 = (\varepsilon_l - \varepsilon_{l'})(\varepsilon_l^* - \varepsilon_{l'}^*)$. We can derive Ω^{D*} and Σ^D in (4) as follows.

$$\Omega_\nu^{D*} = \frac{\partial F^D}{\partial\varepsilon_\nu^*}$$
$$= \sum_{\nu'\in N_\nu}\begin{cases}(\varepsilon_\nu - \varepsilon_{\nu'}) & |\varepsilon_\nu - \varepsilon_{\nu'}| \leq \gamma \\ \gamma\dfrac{(\varepsilon_\nu - \varepsilon_{\nu'})}{|\varepsilon_\nu - \varepsilon_{\nu'}|} & otherwise\end{cases} \quad (6)$$

We obtain the diagonal elements of Σ^D as

$$\Sigma_{\nu,\nu}^D = \frac{\partial^2 F^D}{\partial\varepsilon_\nu\partial\varepsilon_\nu^*} \quad (7)$$
$$= \sum_{\nu'\in N_\nu}\begin{cases}1 & |\varepsilon_\nu - \varepsilon_{\nu'}| \leq \gamma \\ \dfrac{\gamma}{2|\varepsilon_\nu - \varepsilon_{\nu'}|} & otherwise\end{cases}$$

and the non-diagonal elements as

$$\Sigma_{\nu,\nu'}^D = \frac{\partial^2 F^D}{\partial\varepsilon_{\nu'}\partial\varepsilon_\nu^*} \quad (8)$$
$$= \begin{cases}-1 & |\varepsilon_\nu - \varepsilon_{\nu'}| \leq \gamma \\ -\dfrac{\gamma}{2|\varepsilon_\nu - \varepsilon_{\nu'}|} & otherwise\end{cases}$$

A pseudo-code of the complete reconstruction is given under Algorithm 1. Recently, we extended our framework from [16] to a more general class of function [19] (which includes the Huber function as one particluar instance). In this paper, we present a more elaborate evaluation of the whole framework and we test this framework in a more challenging case study with biomedical data.

IV. Results

We performed a large number of simulations with artificial objects and breast phantom data under different antenna configurations. In these experiments, we simulated TM- and TE-polarized scattered field measurements at different frequencies with additive white Gaussian noise and signal-to-noise ratio (SNR) of 30 dB.

We compared three different regularizations: MS [8], SRVP [12] and the proposed method. To keep the 3D forward problems well-conditioned, the constraints on the permittivity were imposed as $1 < Re(\varepsilon) < 10$, $-10 < Im(\varepsilon) < 0$ for piecewise constant objects and $1.0 < Re(\varepsilon) < 55.0$, $-50.0 < Im(\varepsilon) < 1.0$ for the breast phantom. In all the experiments, we used a stabilized bi-conjugate gradient Fast Fourier Transform (BICGSTAB-FFT [20]) forward solver to accelerate the calculations. The computation time is similar for all three considered regularizations provided that equal numbers of antennas are used. Reducing the number of data points
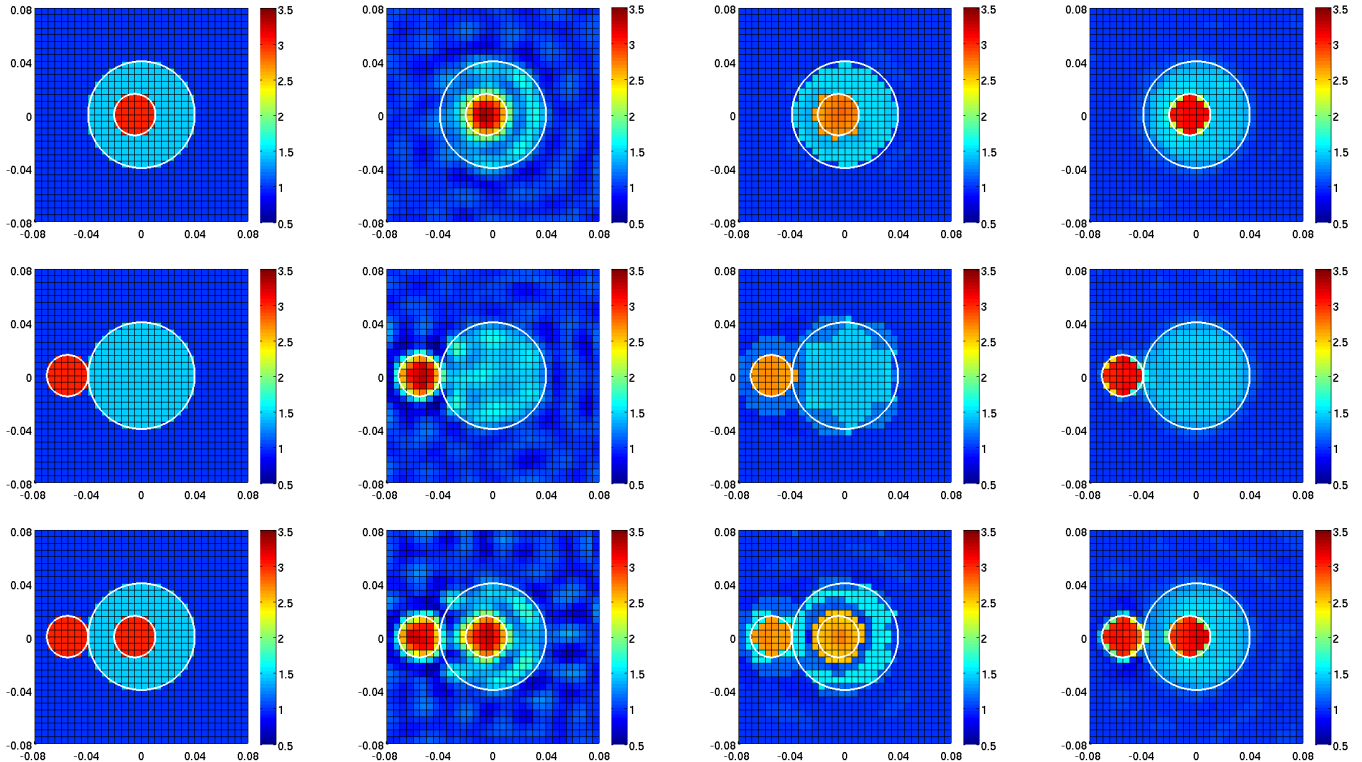
Fig. 1. Real parts of the complex permittivity profile of different methods for three targets from Fresnel database. From left to right: original, MS [8], SRVP [12] and the proposed Huber regularization. From top to bottom: FoamDielInt; FoamDielExt and TwinDiel targets.

is of interest in terms of computation time. We optimize the regularization parameter μ and the parameter γ of the proposed regularization experimentally. For piece-wise constant objects $\gamma = 0.1$ is a good choice and for continuous profiles (like in biomedical cases) a smaller $\gamma = 0.008$ should be used. For the regularization parameter μ we obtained the same optimal value ($\sim 1e-4$ in 2D and $\sim 1e-6$ in 3D) for different targets and different antenna configurations. Our simulations were performed on a sixcore Intel i7 980x processor (3.33GHz) with 24GByte memory.

A. Piecewise constant objects in 2D

We consider different targets and antenna configurations in accordance with the 2D Fresnel database [21], for which we simulate TM- and TE-polarized scattered field measurements at 4GHz. We used three inhomogeneous targets from the Fresnel database: FoamDielInt, FoamDielExt and TwinDiel, shown in Fig. 1 and described in [21]. The antenna positions are equally spaced on a circle with radius 1.67 m. The scattering object is positioned in the center of this circle, see Fig 2. We use 8 equally spaced transmitting antennas, each with two polarizations (TM and TE), and different numbers of receiving antennas, ranging from 16 to 241, resulting in a data vector $\mathbf{e}^{meas}$ of length N^d ranging from 768 to 11568 complex numbers.

All reconstructions start from a 0.16×0.16 m^2 domain $\mathcal{D}$ filled with air as an initial estimate of the permittivity. This

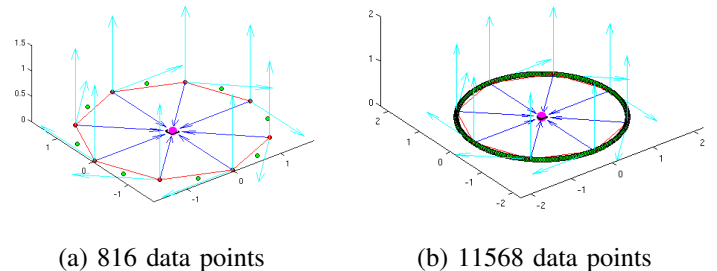(a) 816 data points   (b) 11568 data points

Fig. 2. Two dipole configurations with antenna positions (dots) on a circle with radius 1.67m. The arrows in two orthogonal directions indicate transmitting dipoles. The hightlighted region in the center indicates the reconstruction domain $\mathcal{D}$.

square is chosen as the reconstruction domain in the inverse solver and is discretized in 32×32 square inverse problem cells, yielding a total of 1024 permittivity unknowns. The edge size of an inverse problem cell is 5 mm, which roughly corresponds to 15 inverse problem cells per wavelength λ_0.

With our method (and similarly with other methods), the reconstruction using 768 data points takes less than 5 minutes while around 2 hours are needed using 11568 data points. For the more complex TwinDiel target, the reconstruction takes around 10 mins with 768 data points and 3.5h with 11568 data points.

Reconstruction error	Foamdielint	Foamdielext	TwinDiel
MS	0.067	0.076	0.094
SRVP	0.057	0.065	0.13
Huber	0.055	0.055	0.063

TABLE I
RECONSTRUCTION ERRORS IN THE PERMITTIVITY ESTIMATION OF
FRESNEL DATABASE EXAMPLES FOR DIFFERENT METHODS AND THE
CONFIGURATION FROM 768 DATA POINTS.

To evaluate the quality of the permittivity reconstructions, the reconstruction error R is defined as

$$R = \frac{\parallel \boldsymbol{\varepsilon}^{scat} - \boldsymbol{\varepsilon}^{exact} \parallel^2}{\parallel \boldsymbol{\varepsilon}^{exact} \parallel^2} \qquad (9)$$

which expresses the normalized squared difference between the exact and reconstructed permittivity values on the grid. TABLE I shows reconstruction errors for MS, SRVP and the proposed method for the three targets. The proposed approach is clearly better than the other two, especially for complex targets like TwinDiel.

Fig. 1 shows the reconstructions with the different methods using 768 data points. The parameters for MS and SRVP were set as proposed by the authors in [22]: $\mu = 0.001$ for MS and $\mu = 3$ for SRVP. The results of MS are over-smoothed as expected. The SRVP results retain sharp edges but the reconstructed edge positions as well as resulting permittivity values deviate from the correct ones. The results with Huber regularization are much closer to the ground truth.

B. Piecewise constant objects in 3D

We simulated imaging of several homogeneous and piece-wise constant 3D objects at 8 GHz. All the piecewise constant targets measured in 3D in our simulations are guaranteed to lie in a $0.1 \times 0.1 \times 0.1 m^3$ cube at the center of a reference frame (see Figure 3). This cube is chosen as the reconstruction domain in the inverse solver and is discretized in $20 \times 20 \times 20$ voxels, yielding a total of 8000 permittivity unknowns. The edge size of an inverse problem cell is 5 mm. This relatively small size of an inverse problem cell should facilitate to reconstruct the curved shapes of the measured targets.

The effect of the particular antenna configuration is simulated by the forward solver. In our simulations, the antenna positions are equally spaced on a sphere with radius $0.2m$. The scattering object is positioned in the center of this sphere. For every transmitter position, the target is illuminated using two different polarizations of the plane wave, one along the azimuthal direction and one along the meridional direction (TM and TE).

We performed experiments with different dipole antenna configurations, including the configuration from [12] (shown in Fig. 3(a)) and much sparser configurations, like in Fig. 3(b), (c). The sparser configurations are very attractive from the point of view of computation time but make the reconstruction problem much more challenging.

The analyzed object, denoted hereafter as Object is a cube with side 22.5mm and permittivity 2.5-1j, which is embedded

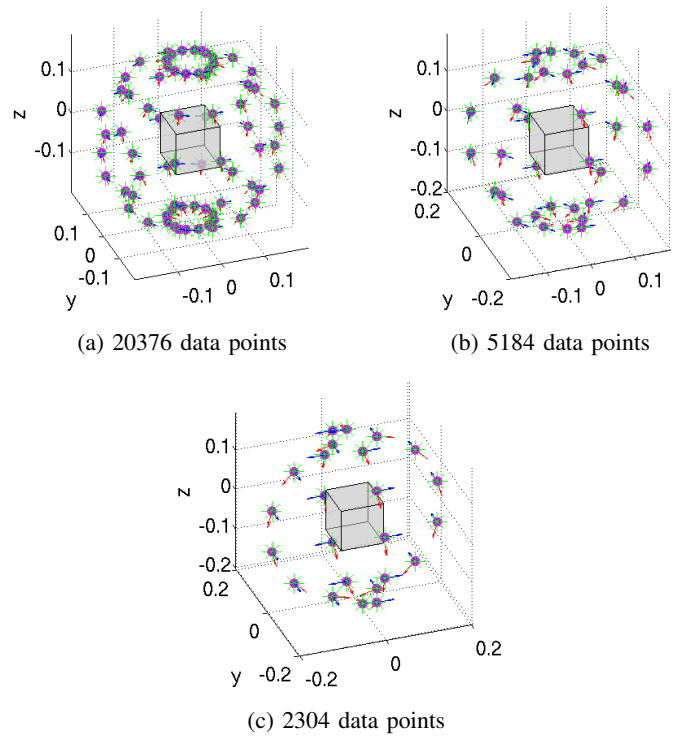(a) 20376 data points

(b) 5184 data points

(c) 2304 data points

Fig. 3. Three dipole configurations with antenna positions (dots) on a sphere with radius 0.2m. The arrows in two orthogonal directions indicate transmitting dipoles. The cube in the center indicates the reconstruction domain $\mathcal{D}$.

in a sphere with radius 30mm and permittivity 1.8. The sphere and the cube are centered at the origin and at the point (-5.6mm,-5.6mm,-5.6mm), respectively (see Fig. 4(a)). Each dipole in the three configurations is used to illuminate the target and the scattered field is measured in every dipole position and along each dipole direction. The configuration in Fig. 3(a) taken from [12] consists of 144 antennas which generate 20736 complex data points. The configuration in Fig. 3 (b) consists of 36 antennas which generate 5184 data points. The sparsest configuration in Fig. 3 (c) consists of 24 antennas which generate 2304 data points.

To reconstruct Object, the dense configuration from Fig. 3 (a) requires 3 hours while the sparsest configuration from Fig. 3 (c) requires only around 40 minutes.

The parameters for MS and SRVP were set as in [22]: $\mu = 0.0001$ for MS and $\mu = 1$ for SRVP. The results in Fig. 4 demonstrate the effectiveness of the proposed method in comparison to the reference ones. SRVP requires much more iterations to arrive at a similar reconstruction quality.

We also evaluate the quality of the permittivity reconstructions based on (9). The results in TABLE I show that the proposed method yields a much lower reconstruction error than the two reference methods MS and SRVP, for the two analyzed targets.

C. Breast phantom data

Here we deal with a more challenging problem: estimation of the permittivity profile in biological tissues, which is no

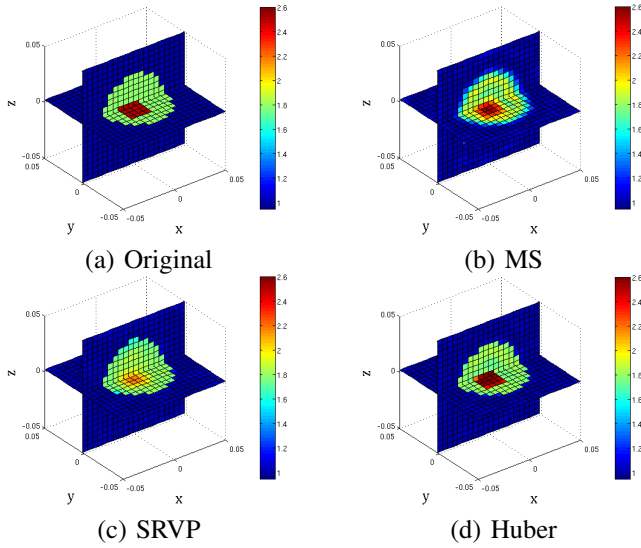(a) Original   (b) MS

(c) SRVP   (d) Huber

Fig. 4. Real parts of the complex permittivity profile and antenna configuration from Fig. 3 (b) in 12 iterations for MS and Huber regularization and 22 iterations for SRVP.

Configuration	MS [8]	SRVP [12]	Huber
20736 data points	0.0588	0.0543	0.0164
5184 data points	0.0713	0.0734	0.0259
2304 data points	0.0826	0.1000	0.0373

TABLE II
RECONSTRUCTION ERRORS IN THE PERMITTIVITY ESTIMATION OF THE
ANALYZED 3D OBJECT WITH DIFFERENT ANTENNA CONFIGURATIONS.

longer piecewise constant, but rather piecewise continuous. The data are taken from Numerical Breast Phantoms Repository (http://uwcem.ece.wisc.edu/home.htm). The original high-resolution MRI data (cell size 0.5mm) are down sampled (to cell size 2.5mm) and a tumor with radius 1cm and permittivity 50-10j is inserted manually. The gray Cuboid in Figure 5 denotes the investigation domain $\mathcal{D}$ where a breast can be placed. The scattering breast is positioned at the center of the domain. This Cuboid is chosen as the reconstruction domain in the inverse solver and is discretized in $24 \times 28 \times 22$ cube inverse problem cells, yielding a total of 14784 permittivity unknowns. The edge size of the inverse problem cell is again 5 mm.

The dipole configuration which is used to generate the data is depicted in Figure 5. It consists of 80 dipoles on a half sphere surface around the domain of the breast with polarizations in two orthogonal directions tangential to this surface. All these dipoles are used to sample the field, but only 64 of them (indicated with the larger green dots) are used to illuminate the phantom because of memory limitations at 2 GHz (increasing the number of illuminations increases the size of the Jacobian matrix too much). For every transmitter position, the target is illuminated using two polarizations of the plane wave, one along the azimuthal direction and the other along the meridional direction. This yields a total of $N^D = 5120$ data points.
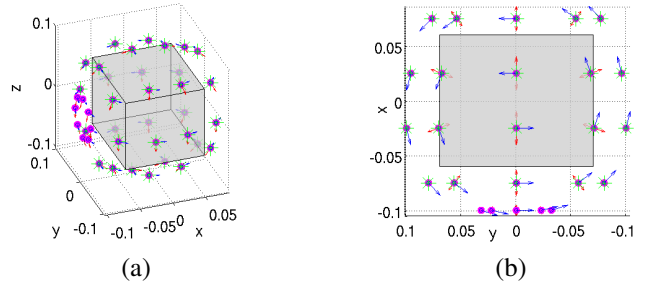

(a)   (b)

Fig. 5. A dipole configuration with antenna positions (dots) on a half sphere with radius 0.2m. The arrows in two orthogonal directions indicate transmitting dipoles. The cube in the center indicates the reconstruction domain $\mathcal{D}$. (a)xyz view; (b) xy view.
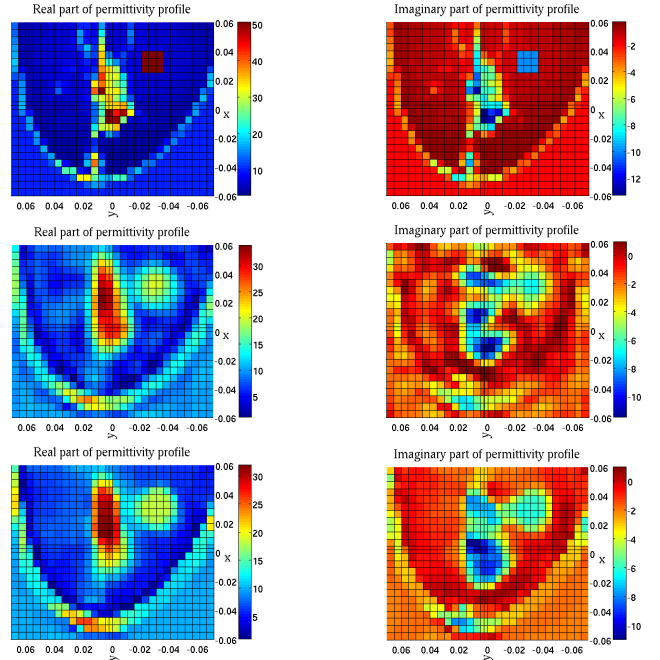

Fig. 6. Breast phantom reconstruction showing the real parts (left) and imaginary parts (right) of the complex permittivity profile. Top: original ground truth data; middle: MS reconstruction; Bottom: Proposed method.

Since SRVP is not suitable for reconstructing other than piecewise constant objects, we compare our approach only to MS regularization in this case study. Both methods start from a domain $\mathcal{D}$ filled with liquid and assume 10-2j as the initial estimate of the permittivity. As we mentioned before, we only have $N^{\mathcal{D}} = 5120$ data points. This means that the problem is heavily under-determined and the regularization and subspace preconditioning are indispensable. To test the abilities of the method, we perform a complete blind reconstruction, i.e. we do *not* use knowledge of the breast contour, which is sometimes suggested in the literature microwave breast cancer imaging. Hence, in our case, the initial estimate is just the uniform background medium. The tolerance for the BICGSTAB (biconjugate gradient stabilized method) iterative routine is set to 10^{-3}. With our method (and similarly for

MS) under configuration in Fig 5 with 5120 data points, the reconstruction takes less than 1 hour. The regularization parameter for MS was set to $\sim 1e-4$ as was suggested by the authors in [12].

Figure 6 shows the real and imaginary parts of one slice from breast phantom data of the reconstructed permittivity profile on a $24 \times 28 \times 22$ grid (cell size 5 mm). The results of MS regularization are again somewhat oversmoothed, which is especially visible in the reconstructed breast contour in the imaginary part. The shape of the breast and the tumor are clearly better reconstructed by the proposed Huber regularization method.

V. CONCLUSION

In this paper, we introduced a new method for convex optimization in the complex domain for two-dimensional and three-dimensional quantitative microwave tomography. In particular, starting from the robust Huber function we derived a discontinuity adaptive regularization that can be used within a Gauss-Newton optimization scheme. The results show a significant improvement over recent related methods, especially under sparse measurements, saving computation time. The method is able to reconstruct the spatial complex permittivity distribution in biological objects from blind reconstruction at one single frequency, thereby overcoming difficulties with the dispersive nature of body tissues. Numerical results indicate the potentials of the method for breast tumor detection even though a thorough analysis for this challenging problem still needs to be done.

REFERENCES

[1] E. Fear, X. Li, S. Hagness, and M. Stuchly, "Confocal microwave imaging for breast cancer detection: localization of tumors in three dimensions," *Biomedical Engineering, IEEE Transactions on*, vol. 49, no. 8, pp. 812 –822, aug. 2002.

[2] E. Zastrow, S. Davis, and S. Hagness, "Safety assessment of breast cancer detection via ultrawideband microwave radar operating in swept-frequency mode," in *Antennas and Propagation Society International Symposium 2006, IEEE*, july 2006, pp. 721 –724.

[3] T. Henriksson, N. Joachimowicz, C. Conessa, and J.-C. Bolomey, "Quantitative microwave imaging for breast cancer detection using a planar 2.45 ghz system," *Instrumentation and Measurement, IEEE Transactions on*, vol. 59, no. 10, pp. 2691 –2699, oct. 2010.

[4] D. Winters, J. Shea, P. Kosmas, B. Van Veen, and S. Hagness, "Three-dimensional microwave breast imaging: Dispersive dielectric properties estimation using patient-specific basis functions," *Medical Imaging, IEEE Transactions on*, vol. 28, no. 7, pp. 969 –981, july 2009.

[5] D. Winters, B. Van Veen, and S. Hagness, "A sparsity regularization approach to the electromagnetic inverse scattering problem," *Antennas and Propagation, IEEE Transactions on*, vol. 58, no. 1, pp. 145 –154, jan. 2010.

[6] J. D. Shea, P. Kosmas, B. D. V. Veen, and S. C. Hagness, "Contrast-enhanced microwave imaging of breast tumors: a computational study using 3d realistic numerical phantoms," *Inverse Problems*, vol. 26, no. 7, p. 074009, 2010.

[7] J. D. Shea, P. Kosmas, S. C. Hagness, and B. D. Van Veen, "Three-dimensional microwave imaging of realistic numerical breast phantoms via a multiple-frequency inverse scattering technique," *Medical Physics*, vol. 37, no. 8, pp. 4210–4226, 2010.

[8] J. D. Zaeytijd and A. Franchois, "Three-dimensional quantitative microwave imaging from measured data with multiplicative smoothing and value picking regularization," *Inverse Probl.*, vol. 25, no. 2, p. 024004, 2009.

[9] A. Abubaker and P. Van Den Berg, "Total variation as a multiplicative constraint for solving inverse problems," *IEEE Trans. Image Process.*, vol. 10, no. 9, pp. 1384 –1392, Sep 2001.

[10] P. Lobel, C. Pichot, L. Blanc-Feraud, and M. Barlaud, "Microwave imaging: Reconstructions from experimental data using conjugate gradient and enhancement by edge-preserving regularization," *Int. Journal of Imaging Syst. and Technol.*, vol. 8, no. 4, pp. 337–342, 1997.

[11] P. Lobel, L. Blanc-Fraud, C. Pichot, and M. Barlaud, "A new regularization scheme for inverse scattering," *Inverse Problems*, vol. 13, no. 2, p. 403, 1997.

[12] J. De Zaeytijd, A. Franchois, and J. Geffrin, "A new value picking regularization strategy - application to the 3-D electromagnetic inverse scattering problem," *IEEE Trans. Antennas Propag.*, vol. 57, no. 4, pp. 1133 –1149, April 2009.

[13] P. Mojabi and J. LoVetri, "Enhancement of the Krylov subspace regularization for microwave biomedical imaging," *IEEE Trans. Med. Imaging*, vol. 28, no. 12, pp. 2015–2019, 2009.

[14] A. Golnabi, K. Paulsen, P. Meaney, and S. Geimer, "Comparison of no-prior and soft-prior regularization in biomedical microwave imaging," *Journal of Medical Physics*, vol. 36, no. 3, pp. 159–170, 2011.

[15] A. Fhager, M. Gustafsson, and S. Nordebo, "Image reconstruction in microwave tomography using a dielectric Debye model," *IEEE Trans. Biomed. Eng.*, vol. 59, no. 1, pp. 156 –166, Jan 2012.

[16] F. Bai, A. Pizurica, S. Van Loocke, A. Franchois, D. De Zutter, and W. , Philips, "Quantitative microwave tomography from sparse measurements using a robust huber regularizer," in *In IEEE Int. Conf. Image Processing (ICIP)*, October 2012, pp. 2073–2076.

[17] S. Van den Bulcke and A. Franchois, "A full-wave 2.5d volume integral equation solver for 3d millimeter-wave scattering by large inhomogeneous 2d objects," *Antennas and Propagation, IEEE Transactions on*, vol. 57, no. 2, pp. 535 –545, feb. 2009.

[18] R. Fletcher, *Practical methods of optimization; (2nd ed.)*. New York, NY, USA: Wiley-Interscience, 1987.

[19] F. Bai, A. Pizurica, S. Van Loocke, A. Franchois, D. De Zutter, and W. , Philips, "Weakly convex discontinuity adaptive regularization for microwave imaging," 2012, submitted.

[20] H. A. van der Vorst, "Bi-cgstab: a fast and smoothly converging variant of bi-cg for the solution of nonsymmetric linear systems," *SIAM J. Sci. Stat. Comput.*, vol. 13, no. 2, pp. 631–644, Mar. 1992. [Online]. Available: http://dx.doi.org/10.1137/0913035

[21] J. Geffrin, P. Sabouroux, and C. Eyraud, "Free space experimental scattering database continuation: experimental set-up and measurement precision," *Inverse Problems*, vol. 21, no. 6, p. S117, 2005.

[22] S. Van den Bulcke, "A 2.5D electromagnetic quantitative inverse scattering technique to visualize concealed objects using millimeter waves," monograph, Ghent University. Faculty of Engineering, 2010.

ACKNOWLEDGMENT